THE JOURNAL OF PHYSICAL CHEMISTRY C

Article

Cite This: J. Phys. Chem. C 2017, 121, 28106−28116

pubs.acs.org/JPCC

Carbon Dots from a Single Source Exhibiting Tunable Luminescent Colors through the Modification of Surface Functional Groups in ORMOSIL Films

Dipsikha Bhattacharya,[†] Manish Kumar Mishra,[†] and Goutam De*

Nano-Structured Materials Division, CSIR−Central Glass and Ceramic Research Institute, 196, Raja S. C. Mullick Road, Kolkata 700032, India

Supporting Information

ABSTRACT: A simple strategy to fabricate carbon dots (CDs) incorporated organically modified silica (ORMOSIL) films exhibiting tunable tricolor emission has been accomplished. First, the green-emitting CDs with excitation-independent nature and high quantum yield were prepared from *o*-phenylenediamine in ethanol by solvothermal method. These CDs after purification were dispersed in ORMOSIL sol, and their photoluminescence wavelengths were tuned to three intense luminescent colors (orange, yellow, and green) by adjusting the pH of the sol. It was observed that with pH tuning the functional groups residing on surface-passivated CDs are undergoing chemical modifications, and accordingly the PL emission of CDs in ORMOSIL sol systematically changes to orange, yellow, and green emissions, respectively. Interestingly, the structure of such surface-modified CDs can be well-preserved in the ORMOSIL film-matrix with substantial concentration to obtain the above tricolor luminescent films on glass. A systematic X-ray photoelectron spectroscopy study revealed that the blue shifting in triluminous films (from 560 to 510 nm) with pH increment was originated due to the deprotonation of the surface groups (−CONH− → −CO(N$^-$)−; −NH$_3^+$ → −NH$_2$) associated with the CDs. The plausible mechanism behind the rationalization of pH-triggered engineering of surface-passivated CD-ORMOSIL sols and their confinement in films has been explored.

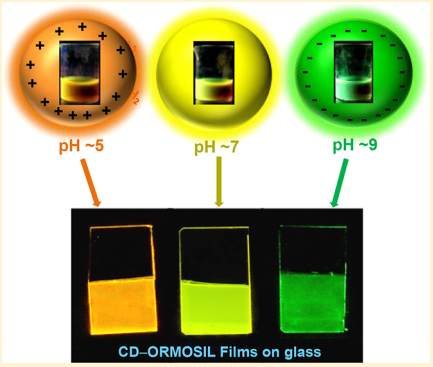

1. INTRODUCTION

Luminescent carbon dots (CDs), an inexpensive emerging nanolight, have flourished as successful probes for bioimaging, drug delivery, and optoelectronic applications by virtue of its bright photoluminescence, biocompatibility, and photostability.[1−3] In the past decade, photoluminescent quantum yields (QYs) of color-emitting CDs have been greatly improved through various chemical methods, such as heteroatom doping, surface passivation, or surface engineering.[4,5] In addition, it is observed that most of the reported CDs to date have excitation-dependent photoluminescence (PL) behavior.[6−8] Of late, efficient long-wavelength-emitting CDs (orange and red) with excitation-independent behavior are apparently preferred for practical applications; however, they are scarce in the literature due to the lack of effective synthesized methods and ambiguous luminescence mechanism.[8−11] Recently, Lin et al.[12] reported three types of tricolor-emitting CDs (blue, green, and red) with excitation-independent PL nature and high QYs using three different isomers of phenylenediamine as precursors, where the observed red shift was attributed due to the quantum size effects and the nitrogen content of the CDs. Additionally, full-color-emitting CDs (from blue to red emission) have been synthesized by other groups,[9,13,14] and they ascribed the observed red shift of emission as due to surface defect states and incorporation of oxidized species. Very recently, Yu et al. reported solvent-dependent full-color generations (green to red emission) from an excitation-independent single green-emitting CD, where the multicolored emissions of single CDs in various solvents were observed due to the inherent "solvatochromism" effect.[15] To date, it is also notable that most of the reported multicolored CDs have been synthesized either from different precursors[12] or by using complicated separation techniques.[9,13−15] Recently, a novel work on synchronous tricolor emission from single component quantum-dot (QD)-based nanocrystal was reported.[16] This single-component-triggered multicolor emission is fascinating because this simple processing can make the production process very cost-effective and beneficial. In addition, CDs are mostly available in solution for which they are used in bioimaging, drug delivery, cancer diagnosis, and metal-ion-sensing applications.[1−3,17] However, for solid-state lighting as well as display applications, the major challenging issue is the inherent PL quenching behavior while being transferred to solid-state matrices due to the aggregation, creating severe problem of quantum confinement.[18,19]

Currently, many research communities are more intriguing to fabricate CD-incorporated monoliths or hard adhesive films on glass and flexible substrates with high PL intensity as well as QYs for solid-state optical applications.[20,21] Recently a few

Received: August 11, 2017
Revised: October 31, 2017
Published: November 29, 2017

DOI: 10.1021/acs.jpcc.7b08039
J. Phys. Chem. C 2017, 121, 28106−28116

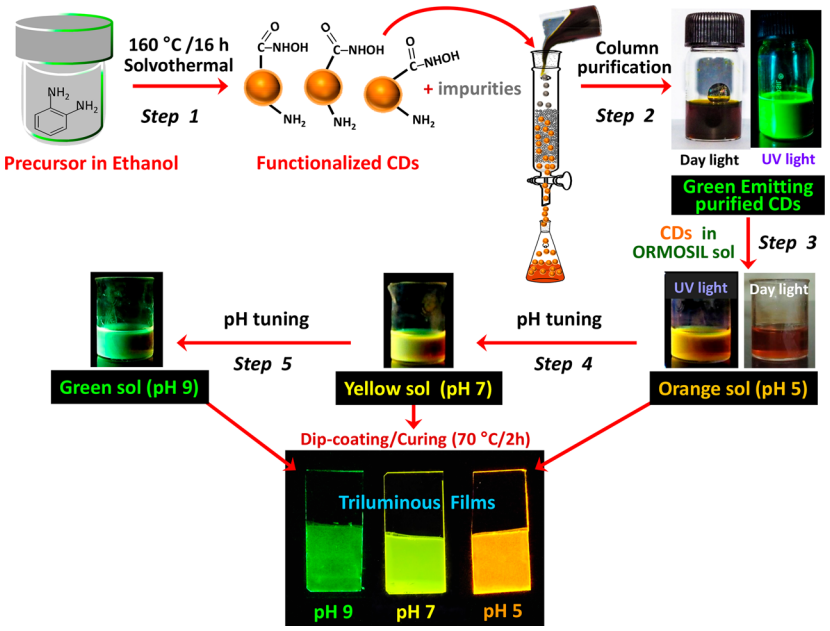

Figure 1. Schematic diagram showing the synthesis, purification, and incorporation of CDs in ORMOSIL matrix to produce tricolor emissive sols as well as films on glass substrate.

multicolored flexible monolithic films have been reported.[12,20−23] For example, tricolor-emitting (red, green, and blue) flexible films were developed using CD-incorporated (poly(vinyl)alcohol (PVA)) polymer matrix exhibiting excitation-dependent nature.[12] Utilizing the excitation-dependent property of CDs, a single CD-PVA flexible film was used to produce three color emitting (cyan, green, and yellow) films with efficient stability.[23] Exploiting the solvatochromic effect of the green-emitting CDs, green-to-red multicolor-emitting flexible films were also fabricated using different solid-state matrices (polymers) with excitation-independent nature.[15] Excluding the last report where the same CDs impart multicolor stable emissions while incorporated in various matrices,[15] the fabrication of multicolor emissive films from single-color-emitting CDs as well as embedment in transparent solid matrices is not yet reported. In most of the available reports, different emissive CDs have been separately prepared and incorporated in the polymer matrices.[12,14−16]

Likewise, CD-incorporated free-standing flexible films exhibiting tricolor PL emission through in situ one-pot carbonization of organic precursor molecules in polymer matrices has been reported.[24] In general, we cannot rule out the possibility of existing undecomposed precursor molecule or impurity during in situ fabrication of CDs inside a polymeric matrix that may be disadvantageous in long-term stability. Furthermore, as an effective alternative for flexible films, dielectric hosts as well as films such as ZrO_2-,[25] TiO_2-,[26] and SiO_2-based[27] matrices have also obtained striking interest as support materials for QD/CD-incorporated films with utmost PL and QY stability. Recently, silica-based organic−inorganic hybrid was attracting emerging attention as solid-state matrices, where a highly luminescent CD-incorporated flexible free-standing film was reported with mesoporous organic/inorganic architecture.[28] Very recently, strongly luminescent CD@SiO_2 composite gels have been reported where the aggregation in the solid state was intelligently conquered.[29] However, the development of hard, transparent fluorescent films using organic−inorganic silica matrices remains relatively unexplored. In this regard, it has been established that organically modified silica known as ORMOSIL[28,30−34] can be the best choice for stabilization of photoluminescent QDs,[27] CDs,[30] and composite[31,32] nanoparticles to obtain hard, transparent, inexpensive fluorescent films on glass and plastic substrates for optical applications. Actually, ORMOSIL matrix due to its inherent inorganic−organic hybrid functional properties stabilizes the CDs from agglomeration both in the sol as well as in the film. Additionally, ORMOSIL has high adhesion capability, transparency, robustness, and nonreactive nature, which do not hamper the pristine properties of CDs.

This work reports the fabrication of hard and transparent films exhibiting tunable tricolor light emission (orange, yellow, and green) through an assembly of green-emitting CDs and ORMOSIL sol via pH tuning. The different luminescence emission could be produced from a single variety of CDs through its surface modification. First, green-emissive CDs with excitation-independent nature were prepared from *o*-phenylenediamine (*o*-PDs) exhibiting high PLQY. The purified green-emitting CDs were then incorporated in ORMOSIL sol to obtain orange-, yellow-, and green-emitting sols by simple pH tuning. Afterward, these stable triluminous sols were utilized to prepare tricolor luminescent films on glass substrates with stable PL and high QYs (detailed description given in Figure 1) by dip-coating technique, followed by curing.[27,30,31,33] It is noteworthy here that the same CD-ORMOSIL sol could produce tricolor emission (orange → yellow → green) with increasing pH values, signifying the changes in surface functional groups associated with CDs producing diverse surface states. To the best of our knowledge, this is the first report of pH-responsive tricolor emissive CD-ORMOSIL sols that were intelligently preserved as hard and transparent films without sacrificing their inherent PL characteristics.

2. EXPERIMENTAL SECTION

2.1. Materials. Reagent-grade of *o*-PD, tetraethylorthosilicate (TEOS), ethyl triethoxysilane (ETES), tetrabutyl ammonium hydroxide (TBAH), and quininesulfate dihydrate

DOI: 10.1021/acs.jpcc.7b08039
J. Phys. Chem. C 2017, 121, 28106−28116

were purchased from Sigma-Aldrich. Absolute EtOH (99.99%), *n*-butanol (99.99%), and *n*-hexane (99.99%) were received from Merck, India. Soda-lime and silica glass slides for coating deposition and silica gel (60−120 mesh) for normal-phase column chromatography were purchased from Riviera and Sisco research laboratory Pvt. Ltd. India. Commercially available silicon wafer (one-side polished; P-type) was used to record the GIXRD pattern of drop-casted CDs and film fabrication to measure the thickness by cross-sectional FESEM.

2.2. Synthesis of Organically Modified Silica (ORMOSIL) Sol. To prepare the ORMOSIL sol, TEOS and ETES in a molar ratio of 2.33:1 have been taken in a round-bottomed flask containing 14.625 g *n*-butanol and stirred for proper mixing. To this, a mixture of catalytic amount of 1(N) hydrochloric acid, that is, HCl (0.565 g), water (5.45 g), and methanol (1.43 g), was added and stirred for another 30 min. The above resultant mixture was refluxed at 80 °C for 90 min and allowed to cool at room temperature. The obtained sol was aged in a refrigerator for 24 h under closed condition at ±5 °C temperature. The final equivalent SiO_2 content of the sol was 15.1 wt %. The aged ORMOSIL sol was used to prepare CD-incorporated sols at room temperature (25 ± 1 °C).

2.3. Synthesis of Green-Emitting CDs in Ethanol. Functionalized green-emitting CDs were synthesized from *o*-PD in ethanol by the solvothermal method. In a 25 mL beaker, *o*-PD (0.14 g) was first dissolved in 14 mL of ethanol and then stirred for 30 min until a clear yellow-colored solution was obtained. This solution was then transferred into a poly(tetrafluoroethylene)-lined autoclave, and this final solution was heated to 160 °C in an oven for 16 h. After cooling to room temperature naturally, dark-brown-colored dispersion was obtained. These CDs were then purified with normal-phase column chromatography using silica gel (60−120 mesh)[13] as a stationary phase and mixtures of *n*-hexane and ethanol (96:4 v/v) as mobile phase. It showed green emission (λ_{ex} = 365 nm), indicating the formation of CDs (Figure S1; Supporting Information). Column-purified CDs dispersed in *n*-hexane/ethanol mixture were concentrated by removing the solvents in a rotary evaporator and further dried in oven at 50 °C for 48 h. Finally, 0.035 g of purified powder CDs was collected. These purified CDs were used for characterization and experimental studies.

2.4. Fabrication of Tricolor Emitting CDs Incorporated ORMOSIL Sols and Films. First of all, for the synthesis of the pH-responsive tricolor-emitting sols as well as films, powder CDs (0.0062 g) and ORMOSIL sol (4 g; ORMOSIL contains ∼0.6032 g equivalent SiO_2) were mixed in ratios (equivalent SiO_2/CD ≈ 100:1 w/w) and the solution was stirred for 30 min to obtain a homogeneous sol. This CD-incorporated ORMOSIL sol appeared as a reddish-orange transparent solution (Figure S2a) and showed a bright-orange color emission (λ_{ex} = 365 nm; Figure S2b), and the pH of this sol was pH ∼5, that is, mildly acidic. Yellow and green emissive sols were prepared by increasing the pH of orange-emitting CD-ORMOSIL sol to 7 and 9, respectively (Figure S2c,d). TBAH (an organic base) was used for pH tuning of sol. Finally, these orange, yellow, and green emissive sols were employed for the fabrication of hard, transparent, and bright luminescent films on glass substrates using dip-coating technique at a withdrawal velocity of 21 cm min^{-1}. Similar coatings on Si-wafer were also prepared for characterization purpose. All coatings were cured at 70 °C for 2 h.

2.5. Characterization. The physicochemical and photophysical properties of the pristine CDs and CD-incorporated sols and films were characterized by transmission electron microscopic (TEM), X-ray diffraction (XRD), small-angle X-ray scattering (SAXS), Fourier-transformed infrared (FT-IR), X-ray photoelectron spectroscopy (XPS), zeta potential, UV−visible, PL, and PL decay lifetime (TCSPC) measurements. UV−visible absorption and emission spectra of the CDs and films were recorded with Cary 50, Varian, and PTI QM-30 spectrometers, respectively. FT-IR spectra of the CDs and scratched-off film samples were recorded (KBr pellet method) using a Nicolet 380 FT-IR spectrometer with 200 scans (2 cm^{-1} resolution) for each sample. High-angle XRD measurements (using a grazing incidence angle of X-ray at 0.3°) and transmission SAXS measurements (in ethanol) of purified CDs were performed with a Rigaku Smart Lab X-ray diffractometer operating at 9 kW (200 mA; 45 kV) using Cu−Kα (λ = 1.5405 Å) radiation. Rigaku nanosolver software was used for the evaluation of particle-size distribution from SAXS data. TEM measurements were carried out with a Technai G^2-30ST (FEI, Eindhoven, The Netherlands) operating at 300 kV. For this purpose, ultrasonically dispersed CDs in ethanol were placed on carbon-coated Cu-grids and analyzed. Zeta potential measurements of CDs in solutions at different pH values were measured by a Malvern zetasizer. XPS measurements were done on a PHI 5000 Versaprobe II XPS system with an Al Ka source and a charge neutralizer at room temperature, maintaining a base pressure at ∼6×10^{-10} mbar and an energy resolution of 0.6 eV. Thickness of films was measured by surfcorder SE-2300 profilometer (Kosaka Laboratory, Japan). The cross-sectional thickness of the CD-ORMOSIL film was measured using a ZEISS SUPRA 35VP (Oberkochen, Germany) field-emission scanning electron microscope (FESEM). For this purpose, films deposited on silicon wafer were used. The pencil hardness of coatings was measured by ASTM D3363 specifications using a BYK Gardner pencil hardness tester, and adhesion of the films on glass substrates was evaluated using the method as per ASTM D3359 cross-cut tape test. The ultimate power falling on 0.5 × 0.5 $in.^2$ film was measured by a UV power puck (S/N-8000; EIT), and the value was 7 mW cm^{-2}. For this purpose, film was kept 2 cm apart from lamps of 8 W.[30]

Refractive index of CD-ORMOSIL film was measured by spectroscopic ellipsometer (J. A. Woollam). The luminescence decay measurements were performed by time-correlated single-photon counting (TCSPC) method. For decay measurements, samples were excited at 375 nm using a picosecond diode laser (IBH 35 Nanoled-07) at a repetition rate of 1 MHz. The typical fwhm of the system response is ∼200 ps. The fluorescence decays were analyzed using IBH DAS6 software. The quality of fitting was evaluated from the χ^2 value and DW parameters, and the PL decay curves were fitted using a triexponential and biexponential functions. These PL decay kinetics can be clearly analyzed using a multiexponential decay function, as shown in eq 1.

$$I(t) = \alpha_1 \exp(-t/\tau_1) + \alpha_2 \exp(-t/\tau_2) + \alpha_3 \exp(-t/\tau_3) \quad (1)$$

where α_1, α_2, α_3, τ_1, τ_1, and τ_3 are the pre-exponential factors and excited-state fluorescence lifetimes associated with the 1, 2, and 3 numbers of components, respectively. Relative QY measurements of CDs (in ethanol) as well as films were done with respect to 10^{-4} M quinine sulfate in 0.01N H_2SO_4 solution

DOI: 10.1021/acs.jpcc.7b08039
J. Phys. Chem. C 2017, 121, 28106−28116

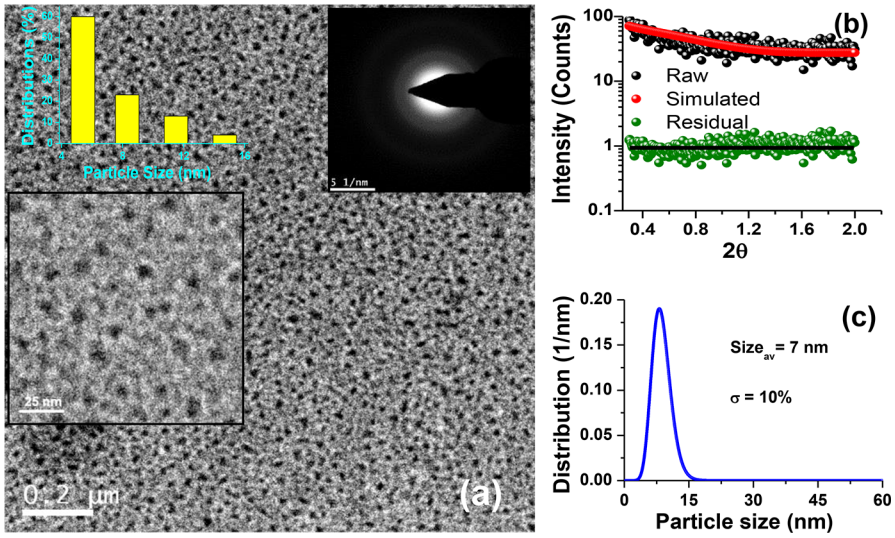

Figure 2. TEM and SAXS studies of purified CDs. (a) TEM image of purified CDs. Insets of panel a show the particle size distribution of CDs (upper left), magnified TEM image (lower left) and SAED pattern (upper right). (b,c) Fitted SAXS pattern and particle size distribution curve obtained from SAXS, respectively.

as a standard. To minimize reabsorption effect, diluted CD solutions as well as films were used for QY measurement. (Detailed information is given in the Supporting Information.)

3. RESULTS AND DISCUSSION

Figure 1 shows the schematic diagram of synthesis procedure of green fluorescent CDs with excitation-independent nature along with the fabrication of tricolor-emitting luminescent films from the CDs incorporated ORMOSIL sols. Previously, Lin et al. has synthesized N-doped CDs via a simple carbonization of triaminobenzene using solvothermal technique at 120 °C.[14] The resultant CDs contained a relatively high abundance of nitrogen-containing functional groups, including amines, amides, and other carbon−nitrogen units like pyridinic and pyrrolic N. The identical nature of carbon source (i.e., *o*-PD) in our synthesis also leads to achieve similar surface functionalization of CDs. However, on the basis of our pH-induced evolution of tricolor emission and several characterizations, we further believe that amino and hydroxamic acid (−CONHOH) groups are predominantly present in our system. Although the presence of amide groups cannot be ruled out,[13−15] its transformation to hydroxamic acid groups is expected[14] due to the prolonged carbonization and oxidation under solvothermal condition (160 °C/16 h). In fact, hydroxamic acid group is playing a major role for evolution of green PL emission through deprotonation at pH 9 owing to its pK_a value ∼8.5. As the pK_a value of amide is 16, deprotonation of amide would not be possible at pH 9. The surface-functionalized CDs showing deep green emission were obtained through a column purification technique. The TEM image (Figure 2a) of the purified CDs shows monodispersed CDs having near-spherical morphology. The size distribution of CDs, as obtained from the TEM image, is given in the inset of Figure 2a. It gives an average size of CDs close to 7.3 nm. A magnified TEM image is also shown in the inset of Figure 2a for clear visualization of CDs. Diffuse rings in SAED pattern acquired from TEM (inset of Figure 2a) indicate that the purified CDs are amorphous in nature.[35,36] Furthermore, to reconfirm the particle size of CDs, transmission SAXS analysis has been performed (Figure 2b,c), and the average particle diameter was found to be 7.0 nm, which is matching well with the average particle size value obtained from TEM. Moreover, these CDs exhibit relatively lower normalized dispersion value, σ (∼10%), signifying the uniform size distribution of the purified CDs. The GIXRD pattern (Figure S3) of these purified CDs shows a broad hump in the range of 16.5−22° 2θ, confirming also its amorphous nature.

The FT-IR analysis has been performed to understand the presence of functional groups present on the CDs before and after purification process, and the results are presented in Figure S4a,b (Supporting Information). It was quite obvious that during the solvothermal carbonization of *o*-PDs, diversely functionalized CDs with ample functionalities were formed through the condensation, polymerization, oxidation, as well as surface passivation phenomena.[13,15,35,36] In both the as-prepared and purified CDs (Figure S4, Supporting Information), the bands at 3400−3200 cm^{-1} are assigned to the stretching frequencies of O−H and N−H groups, ensuring the presence of hydrophilic surface. Both the CDs display C−H vibration at ∼2933 and ∼2840 cm^{-1}. Moreover, stretching vibrations of C═C (1508 cm^{-1}), pyridinic C═N (1590 cm^{-1}), and C−N = (1450 cm^{-1}) groups are observed for these samples, indicating the formation of polyaromatic structures of CDs.[13,37] The existence of stretching vibrations of O−H (∼3400 cm^{-1}), C═O (1620 cm^{-1}), and C−N (1427 cm^{-1})[38] and bending of NH_2 (1591 cm^{-1}, see the magnified view of FT-IR spectra shown in Figure S4b, Supporting Information) in both of the CDs attributed the most likely presence of hydroxamic (−CONHOH) and amine (−NH_2) functional groups. In particular, the band that appeared at 1427 cm^{-1} was the mixed bending vibrations of N−C−H and N−OH groups, corroborating the characteristics of hydroxamic acids.[39] Furthermore, the C−C stretching modes (coupled to N−H bends) were also found at 1217 and 1189 cm^{-1}, indicating successful functionalization with hydroxamic acids.[39] A small peak at 1030 cm^{-1} assigned for N−O stretching vibration was also observed.[40] Along with these peaks, the presence of hydroxamic acid functionalities (−CONH−) was believed to be present in these CDs as the observed C═O band (1620 cm^{-1}) in these CDs has appeared at comparatively lower wavenumber

DOI: 10.1021/acs.jpcc.7b08039
J. Phys. Chem. C 2017, 121, 28106−28116

than the normal carbonyl in amides (1680−1630 cm^{-1}). This has happened due to the functionalization of hydroxamic acid groups, as also observed by previous workers.[40,41] This lowering compared with normal amide was due to the carbonyl bond weakening resulting from enhanced electron delocalization of −NH and −OH of hydroxamic (keto form) group, which was very clearly represented by Higgins et al.[41] In addition, the two sharp peaks at ∼1276 and ∼1126 cm^{-1} are assigned to the stretching vibrations of C-NH (aromatic)[34] and C−O−C, respectively. FT-IR studies at the outset confirm decrease in relative intensities of functional groups in the case of purified CDs due to column purification. Nevertheless, the study reveals the existence of a significant amount of amine and hydroxamic acid functionalities on the surface of the purified CDs, as also observed by other groups.[13,14,35,42]

X-ray photoelectron spectroscopy (XPS) is further performed to understand the exact nature of the functional groups associated with the purified CDs. The surface survey spectra of CDs presented in Figure S5a (Supporting Information) contain mainly three peaks C 1s (284.5 eV), N 1s (399.2 eV), and O 1s (530.5 eV), confirming that the sample is mainly consisted of C, N, and O. To further elucidate the contribution of the surface functional groups of CDs, the deconvoluted high-resolution XPS scans of C 1s and N 1s are provided. In the high-resolution spectra, the C 1s can be deconvoluted into seven peaks according to Voigt equation[43] (Figure S5b; Supporting Information), and the characteristic peaks include C═C (sp^2 carbons), C−C (sp^3 carbons), C═N (pyridine), C−N (pyrrole), C−O (attached OH), C═O (carbonyl of hydroxamic group), and $\pi-\pi^*$ interaction (shakeup peak) for C−C bond at 284.35, 285.2, 286.3, 287.0, 288.0, 288.9, and 291.1 eV, respectively.[13,14,44−46] It was observed from the previous reports[42,47] that the hydroxamic acid group stabilized nanoparticles exhibited almost similar binding energy for carbonyl group (C═O).[42,47] It is to be noted that the presence of C═C, C−C, and shakeup peak designate the characteristic of conjugated aromatic systems with surface functional groups.[48] The corresponding deconvoluted N 1s XPS spectrum (Figure S5c; Supporting Information) shows five peaks at 398.86, 400.1, 402.5 eV, 403.4 and 404.67 eV; among these the first three major peaks were assigned for pyridinic-N (C═N) and pyrrolic-N (C−N═)/amide N and $-NH_2$ groups, respectively.[49−52] Moreover, the higher energy peak appeared at 403.4 eV was the characteristic peak of the N−O bonds reflecting the presence of −CONHOH groups.[52] In addition, the small shakeup ($\pi-\pi^*$) peaks for N 1s were also present[51] due to the satellite peaks of N 1s photoelectrons. Thus XPS analysis reveals that these CDs are composed of conjugated polyaromatic structures and most likely contained the −CONHOH and $-NH_2$ functional groups, which is also consistent with the FT-IR results.

It is noteworthy here that our main objective is to fabricate stable multicolor emitting fluorescent films through the modification of surface functionalities of CDs via pH tuning in ORMOSIL sol and followed by film fabrication. For embedment of CDs with retention of its chromophoric structure, we have selected ORMOSIL sol as our organic−inorganic host matrix as this sol have been widely explored as a hard coating as well as fluorescent nanoparticle-embedded transparent films.[28,30] First, the pristine green-color-emitting purified CDs (image shown in Figure S1b, Supporting Information) were mixed with ORMOSIL sol in proper ratios. Because the ORMOSIL sol has been prepared by acid hydrolysis method, the initial pH of the sol remains mildly acidic (pH ∼5) after mixing the solution of CDs. We observed that the green-emitting CDs produce bright-orange fluorescence-emitting ORMOSIL sol (Figure S2b, Supporting Information), reflecting the considerable changes in surface functionalities of CDs. Furthermore, when this orange sol was tuned to pH ∼7 and ∼9 by standard base TBAH, the PL emission of orange sol experienced sequential blue-shifting of emission to yellow and green color. This red-shifting in PL emission was expected to be due to the modification of the active hydroxamic (−CONHOH) as well as protonated amine ($-NH_3^+$) groups associated with CDs in ORMOSIL sol because of their significant protonation in acidic environment (pH ∼5).[53,54] In addition to that, because the CDs are composed of pyridinic N groups, further enhancement in positive charge is possible due to the protonation of these pyridinic N at pH ∼5 in the ORMOSIL environment. When the CD-ORMSOIL sol was adjusted to neutral zone (pH ∼7), the protonated amine ($-NH_3^+$) groups render the matrix with more free NH_2 groups (deprotonated), driving its PL emission toward yellow, retaining the hydroxamic groups more or less undisturbed on CDs (Figure S2c, Supporting Information). But with further pH enhancement (pH ∼9), the proton attached with N is expected to be deprotonated in the ORMOSIL sol medium. It should be noted here that hydroxamic acid group is acting as N acid rather than O acid in aqueous alcohol environment, which is exactly similar to the ORMOSIL medium used in our case.[54−56] Therefore, the whole chemical environment became highly negatively charged with a predominant presence of $[-CON^{(-)}OH]$ groups, and as a result, green PL emission (Figure S2d, Supporting Information) of CDs was observed in CD-ORMOSIL sol.

To confirm the above-mentioned protonation/deprotonation phenomena, we have performed zeta potential measurements of purified CDs in solution at three different pH values 5, 7, and 9. For this purpose, CDs were taken in *n*-butanol−methanol solvent mixture, and acidic water was used to adjust the pH at 5 (same composition used to prepare the ORMOSIL sol). Then, the solution pH was further adjusted to 7 and 9 by the addition of TBAH, as performed for CD-ORMOSIL sol. The changes of zeta potential values measured using these CD solutions are shown in Figure S6 (Supporting Information). It was observed that at pH 5 the zeta potential of CDs was +72.1 mV (Figure S6, Supporting Information). However, when the pH was raised to ∼7, followed by ∼9, the zeta potential was reduced to around +20.8 and −16.4 mV, respectively. Such modifications of surface charges strongly suggest that there must be some changes in functional groups of CDs with increasing pH values.[57,58] At pH 5, most of the amine groups are protonated and giving high positive value of surface charge. With increase in pH to ∼7, zeta potential value was obtained around +20.8 mV due to the reduced number of protonated amine groups. As the pK_a of hydroxamic acid is 8.5, at pH 9 deprotonation of hydroxamic acid (acting as N-acids) was resulted due to the formation of negatively charged functionality on the surface of CDs, leading to a zeta value of −16.4 mV. Therefore, surface charge analysis revealed the structural changes in the surface functional groups of CDs with pH tuning, which is also observed in the ORMOSIL sols, as discussed above. Such modifications of surface functional groups are responsible for the tricolor emission, which has also been further confirmed by the similar PL behaviors of pristine purified CDs in solutions at the three pH values.

DOI: 10.1021/acs.jpcc.7b08039
J. Phys. Chem. C 2017, 121, 28106−28116

It is thus well understood that the structures of CDs can be well-preserved in ORMOSIL matrix due to its cross-linking hybrid network having plenty of condensable silanol groups, and consequently durable luminescent films on glass substrates were obtained. The triluminous, that is, orange-, yellow-, and green-emitting, films fabricated by standard dip-coating and followed by curing are represented as OF, YF, and GF, respectively. It is noteworthy here that the ORMOSIL sol plays a dual role, it stabilizes the surface-functionalized CDs by chemical interaction (mainly H-bonding, as shown in Figure 3),

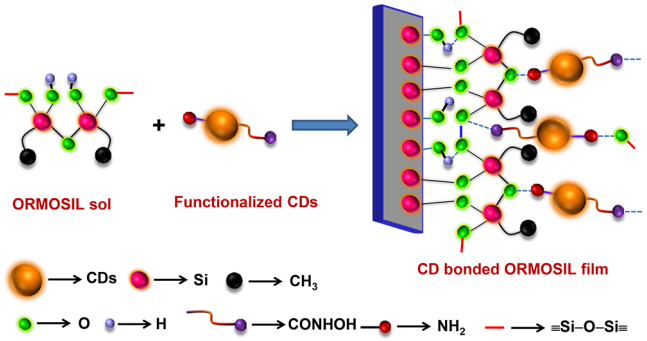

Figure 3. Schematic diagram represents the film fabrication phenomena exploiting the interaction of surface-functionalized CD incorporated ORMOSIL sol and the functionalities (Si−OH) of glass substrate.

and also helps for excellent adhesion with glass surfaces due to the condensation of the ORMOSIL sol-originated Si−OH with the surface −OH groups of glass substrate.[33] The thickness values of the films deposited on glass substrate were measured by a profilometer and found to be ∼1.3 μm (Figure S7, Supporting Information). Almost similar thickness value was also observed through cross-sectional FESEM analysis (thickness ∼1.26 μm, Figure S8, Supporting Information). The adhesion and surface hardness properties of these films were also measured using standard ASTM methods,[27−30] and they were of class 4B and ≥5H, respectively. The refractive index of these CD-ORMOSIL films was found to be 1.462 at 633 nm.

A detailed XPS analysis of CD-ORMOSIL films was undertaken to realize the chemical modifications that occurred, if any, around the CDs when preserved in ORMOSIL environment obtained from precursor sols at different pH values. Figure 4a−c shows the normalized as well as deconvoluted C 1s XPS spectra of three films, that is, OF, YF and GFs. We observed that the relative intensity of C═O group assigned at 288.1 eV decreases from OF to YF and finally becomes nonexistent in GF. The complete disappearance of C═O peak in GF indicates that there may be some deformation occurring in the hydroxamic group at higher pH. Along with this, C 1s spectra (Figure 4) of the films show that the relative intensity of pyridinic C═N peak (∼286.6 eV) remained almost unchanged in intensity from OF to GF. Furthermore, the relative ratio of these two groups (C═N and C═O) was calculated from the integrated area under the curve of the corresponding C 1s spectra (Figure 4a−c). Interestingly, an increasing ratio of C═N to C═O is observed from OF → YF → GF with a blue-shifting in PL spectra. In OF, the amount of C═O is marginally higher than pyridinic N, that is, C═N (C═N/C═O ≈ 0.848:1), while in YF and GF, the reverse order is followed, that is, the amount of C═N was slightly higher in YF (C═N/C═O ≈ 1.16:1), which was almost two fold in the case of GF (C═N/C═O ≈ 2.14:1). Thus we propose that such increasing trend of C═N to C═O ratio (from OF → YF → GF) with increase in pH signifies some deformation of −CONHOH groups present on CDs toward hydroxamate anion [CON$^{(-)}$OH].[56,59,60] Likewise, the deconvoluted N 1s spectra (401.08 eV, Figure 4d,e) experienced considerable amount of decrease in peak intensity from OF to YF. Interestingly the peaks related to the hydroxamic groups are completely absent in GF, indicating the probable chemical transformation of the −CO(NH)OH functional groups with pH tuning, as indicated above. Thus it was evident that the C═N and C═O functionalities associated with −CONHOH are the major driving factors behind the successful attainment of tricolor emission with pH tuning. This phenomenon was almost similar to the previously reported GQDs where similar decreasing pattern was observed for amide carbonyl from the generation of yellow to blue emitting GQDs.[61−64]

Figure 5a depicts the UV−vis absorption spectrum of green-emitting purified CDs showing a single peak at 276 nm along with a shoulder at 304 nm, corresponding to the II−II* transitions of C═C and C═N bonds in aromatic rings.[65]

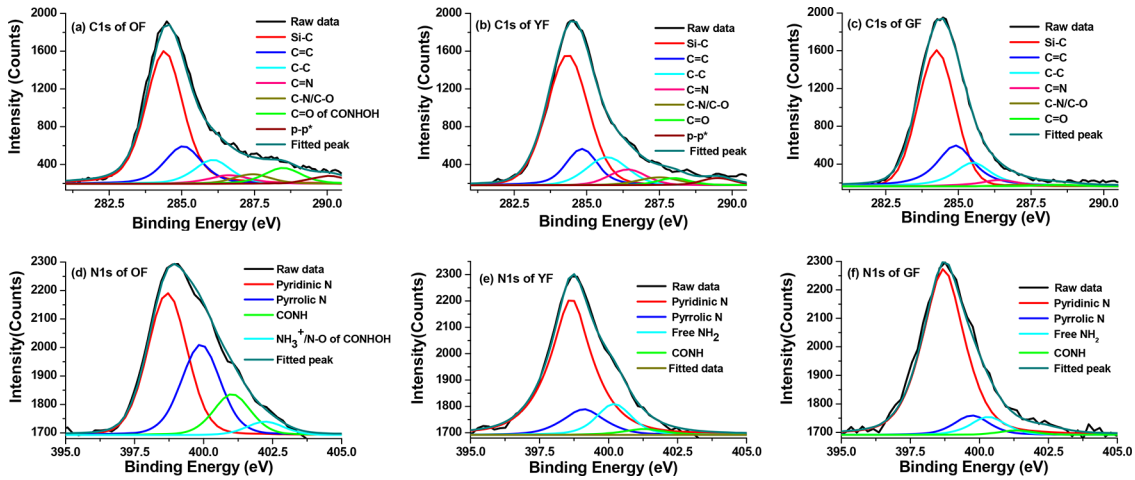

Figure 4. (a−c) High-resolution C 1s spectra of triluminous films demonstrating decrease in C═O bonds of hydroxamic (−CONHOH) groups. (d−f) N 1s spectra reflecting the subsequent decrease of C═O bonds of −CONHOH groups.

DOI: 10.1021/acs.jpcc.7b08039
J. Phys. Chem. C 2017, 121, 28106−28116

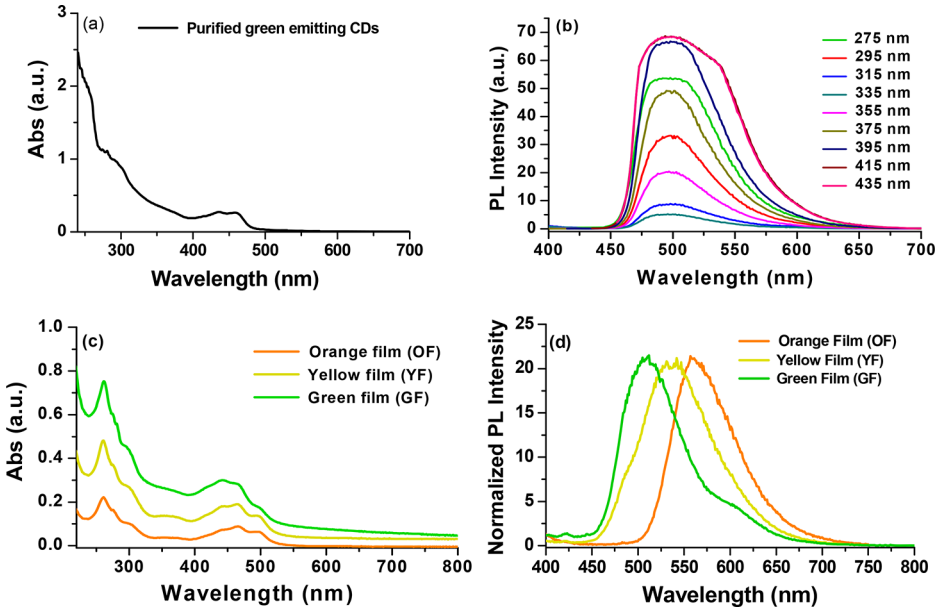

Figure 5. (a) UV−vis spectrum of purified CDs in ethanol. (b) Excitation-independent PL emission of purified CDs in ethanol at 498 nm (excitation wavelengths are from 275 to 435 nm). (c) Characteristic UV−vis spectra of triluminous (orange, yellow, and green) CD-ORMOSIL films prepared at different pH values. (d) Triluminous films showing strong PL emission with negligible overlap at the excitation wavelength 275 nm.

Other two broad shoulders indicating the presence of intrinsic surface states, responsible for strong emission, appeared at 434 and 460 nm.[6,12−14] The PL emission of these purified CDs exhibits deep green luminescence (λ = 498 nm) with excitation-independent nature when excited with different λ_{ex} ranging from 275 to 435 nm (Figure 5b). The emission maximum of green-emitting CDs was observed at 498 at 275 nm excitation, with a PL QY of 55.27%.

With the aim to check the influence of pH values on the PL of purified green-emitting CDs (λ_{ex} = 275 nm) without ORMOSIL matrix, PL emissions of CD solutions (in a similar way as described in zeta potential measurement) were measured at different pH values, and the results are presented in Figure S9. It was observed that at pH ∼5 these green CDs exhibited slightly reddish orange emission with peak maximum at 550 nm while at pH ∼7 a significant blue shifting was observed to 520 nm along with a small additional peak at 480 nm. At pH ∼9 the strong original green-colored emission was reappeared. All of these PL results of pristine green CDs at different pH values are almost similar to the emissions of CDs in ORMOSIL. However, emissions in solutions (without ORMOSIL) were not stable and decayed quickly. In the presence of ORMOSIL environment (sol as well as film) similar PL emissions with long stability were observed. The appearance of similar PL emissions of CDs in solutions, ORMOSIL sols, and films firmly confirmed similar changes of surface functional groups associated with the CDs with respect to the pH values. It is therefore well understood that the same local chromophore around the CDs has been retained in ORMOSIL environment.

After triluminous film fabrication, it has been observed that these films experienced blue-shifted absorption (Figure 5c; λ from ∼478 to ∼456 to ∼445 nm) with increasing pH (5 → 7→ 9) due to the modification of surface functionalities associated with CDs, causing diverse surface states.[13,65,67] Figure 5d depicts the normalized PL emission spectra of these triluminous (OF, YF, and GF) films with emission peaks at 560, 540, and 510 nm, respectively (λ_{ex} = 275 nm). It was shown that the green-emitting CDs exhibit a peak at 498 nm resulting from carbon-core emission, which was significantly red-shifted to 560 nm in OF with relatively reduced in intensity (QY = 17.82), when incorporated in ORMOSIL matrix. Similarly, PL emission is further blue-shifted at ∼540 (yellow emission) and 510 nm (green emission) for YF and GF, respectively, when pH of the sol is further raised. It is believed that the multicolored emissive behavior of these films will be controlled by both the carbon-core and surface domain. The orange color in OF was expected to be originated due to the presence of defect states that produced by the interaction of CDs in acidic ORMOSIL environment (pH ∼5). The PL emission in OF could arise from the surface domain with complete absence of carbon core emission, whereas in the case of YF (pH ∼7), the relatively broader nature of the PL curve suggests that there are substantial contributions of surface-state (∼540 nm) and core-state emissions (∼495 nm). This emission at ∼495 nm may arise from the carbon core due to the facilitated electron−hole recombination, which further controls the surface domain as observed in GF. Thus in GF (pH ∼9) the predominating peak appeared at ∼510 nm with highest intensity and complete disappearance of surface domain, indicating the regeneration of carbon core emission. Therefore, as mentioned before, this pH-tuned PL emission was matched well with the previously observed behavior of CDs, where with increasing pH the fluorescence resulting from the carbon core dominates over the fluorescence from the surface domain observed at acidic pH.[66] It is also noteworthy to mention here that the excitation-independent emission nature of CDs was preserved in three triluminous ORMOSIL films, while PL spectra was taken at different excitation wavelengths (λ_{ex}) (Figure S10, Supporting Information).

The popular PL models proposed for CDs established that surface defects are primarily created through surface oxidation, leading to evolution of surface-state PL emission.[13−15] Nevertheless, in our case, this phenomenon is somewhat different and controlled by the tuning of surface charge of CDs via pH regulation of the system. This controlled surface charge

DOI: 10.1021/acs.jpcc.7b08039
J. Phys. Chem. C 2017, 121, 28106−28116

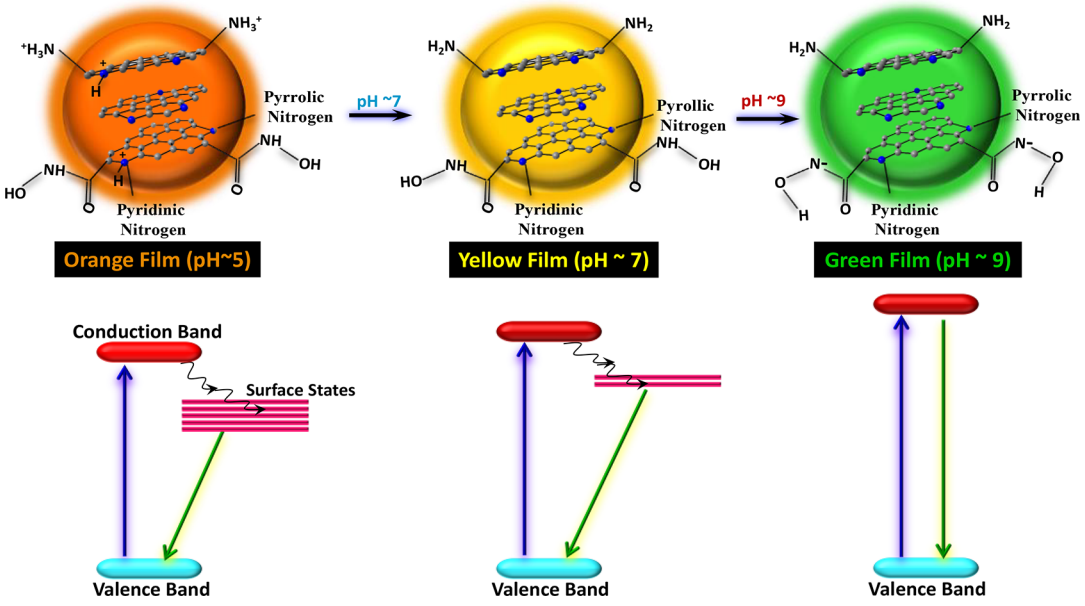

Figure 6. Schematic diagram demonstrating the pH-dependence mechanism of band-gap modifications of CDs in the CD-ORMOSIL solid-state matrix.

tuning allows us to play with PL contribution of both the surface-defect- and carbon-core-related emission, leading to multiple color PL emission. On the basis of the results from XPS and PL analysis, a possible structural model of the pH-sensitive CDs and their triluminous emission states in the ORMOSIL sols and the corresponding films has been illustrated in the schematic diagram (Figure 6). It is noteworthy here that as the pH/pK_a-induced emission changes are mainly associated with the hydroxamic acid, pyridinic N and NH_2 groups, these groups are only highlighted in the schematic diagram, Figure 6 (also in Figure 1), for the simplicity and better understanding. FT-IR and XPS analysis confirmed the presence of polyaromatic structures such as pyridinic, pyrrolic, and graphitic networks in our CDs. It was explained by Dhenadhayalan et al.[66] that electron-withdrawing groups attached to CDs having graphitic/aromatic structures make them electron-deficient. Thus with increase in electron-withdrawing power of the substituent, the PL emission can be tuned from lower wavelength (blue)/high band gap to higher wavelength (red)/low band emission. On the basis of this concept, in the present case, amine- and hydroxamic-group-functionalized CDs containing graphitic, pyridinic, and pyrrolic structure will get protonated at pH 5 and will result in electron-deficient graphitic, pyridinic and pyrrolic structures. It is believed that the protonation will occur at $-NH_2$ and pyridinic nitrogen as their pK_a values are around 5.2 and 4.6, respectively.[55] In addition to this, the electron-withdrawing nature of −CONHOH groups will further facilitate the electron withdraw from the conduction band of the carbon core, thereby preventing the subsequent electron−hole recombination. This hindrance in electron−hole recombination in OF generates pronounced surface defects eventually leading to the predominance of surface-state emission and complete disappearance of core emission.[64−68] When pH of the system is raised to ∼7, protonated amine and protonated pyridinic N will revert back to their unprotonated state; however, the electron withdrawal character of −CONHOH would remain in action and lead to the broad PL spectrum having contribution of both surface-state and core-state emissions. Further rise in pH to 9 leads to complete deprotonation of −NH moiety of hydroxamic acid group (pK_a ∼8.5),[56,59,60] owing to which it loses its electron-withdrawing character and facilitates the electron−hole recombination. This results in the predominance of carbon core emission with the concomitant significant reduction of surface-state emission in the PL spectrum. In fact, XPS of YF and GF (pH ∼7 and ∼9), corroborate the deprotonation along with the formation of [$CON^{(-)}OH$] groups with subsequently decreasing amide bond intensity.

To evidence these triluminous color generation is originated from different emitting centers, the relative QYs for the GF, YF, and OFs were measured with respect to quinine sulfate at 275 nm excitation (Table S1, Supporting Information) and were 36.13, 24.27, and 17.82%, respectively. The decreasing order from GF to OFs (GF > YF > OF) is due to the predominance of direct electron−hole recombination, that is, carbon-core emission over the surface domain.[7,18] As the intensity of PL emission in GF corresponding to carbon-core is higher compared with surface-state-driven emission in OF, it is also reflected in their decreasing order of QYs. The ability to truly tunable luminescence into the higher wavelength region enables new research opportunities for the preparation of multicolor-emitting CDs. Thus the photostability of these films was also checked by irradiating a representative (orange emission) film under UV lamp (λ_{ex} = 254 nm, 8 W) for 4 h (Figure S11, Supporting Information). Although, decrease in PL intensity was initially recorded within 2 h of UV irradiation, thereafter negligible decrease in PL intensity was observed, indicating that these fabricated films possess excellent photostability.

Finally, to understand the participation of core- and defect-related PL emissions in this triluminous color generation, the PL decay lifetime analysis was performed using time-correlated single-photon counting methodology (TCSPC). A gradual increase in decay lifetime was observed from GF to OFs (Table S2, Supporting Information), confirming the presence of localized intermediate energy states in between HOMO−LUMO bands and subsequently increasing the recombination time of exciton in the case of yellow and orange emission.[7] Therefore, the straight as well as curvy nature of logarithmic PL

DOI: 10.1021/acs.jpcc.7b08039
J. Phys. Chem. C 2017, 121, 28106−28116

decay plots (Figure 7) for green, yellow, and orange films (GF, YF, and OFs) confirms the dominant contribution of core- and surface-state emission in the respective films.

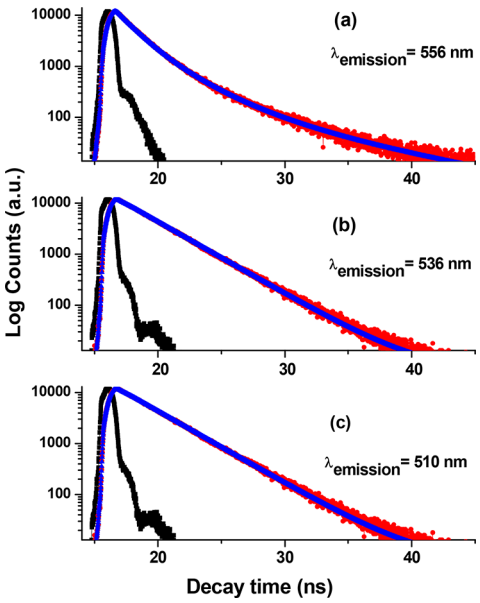

Figure 7. PL decay lifetime spectra of triluminous films obtained at different pHs: (a) orange film, (b) yellow film, and (c) green film.

Basically, these intermediate energy states corresponding to surface defects provide a platform for excited electrons, where it can extend its stay in the excited state before recombination with holes. Therefore, in the case of OF, the decay curve shows triexponential fitting with the highest value. However, from YF to GF, where the surface-state emission tends in decreasing order, the curves exhibit biexponential fitting with considerable lower values. The pattern of PL decay lifetime plot is also an indicator about the participation of surface-state emission. The curvy nature of OF demonstrates the participation of surface state emission, whereas in YF and GF, the straight line decay plots signify the core-state emission of CDs. With increase in surface states (due to the defects in CDs in OF), the nature of logarithmic decay plot changes from straight line to curved type, which indicates that more than one component is involved for the PL decay from the excited state. The pattern of decay lifetime of GF (straight line) was also matched well with the lifetime of pristine green-emitting CDs (Figure S12, Supporting Information), signifying that the PL emission of green-color-emitting CDs was fully controlled by the carbon-core emission of the CDs.

4. CONCLUSIONS

Visually transparent and hard tricolor luminescent films on glass substrates were fabricated by incorporating functionalized CDs into ORMOSIL matrix. Initially green-emitting excitation independent CDs showing high QY were prepared by solvothermal decomposition of *o*-PD. These surface-functionalized CDs were mixed with ORMOSIL sols, and pH modulation yielded orange-, yellow-, and green-emitting hybrid sols. We showed that the sol to transparent film formation does not cause any chromophoric changes around the CDs, and as a result, the luminescent characteristics of these CDs in ORMOSIL films can be well preserved after curing. The detailed surface functional groups associated with the purified CDs and their modifications during pH changes were established in line of the tuning of luminescent characteristics. Therefore, our study paves the way toward the potential fabrication of multicolor emissive films using CDs from a single source. These films may replace metal-based toxic QDs in the application area of LED color converter and luminescent solar concentrator in near future.

■ ASSOCIATED CONTENT

Supporting Information

The Supporting Information is available free of charge on the ACS Publications website at DOI: 10.1021/acs.jpcc.7b08039.

Details of QY measurements (S1). Calculation method of lifetime values (S2). Table representing the analysis of QYs of tricolored films (Table S1). Table representing average lifetime values of three films (Table S2). The digital images of green-emitting CDs under visible and UV light (Figure S1). The digital images of CD-ORMOSIL sols (Figure S2). XRD pattern of purified CDs (Figure S3). FT-IR spectra of solution CDs before and after purification (Figure S4). Survey scan and high-resolution XPS spectra of CDs (Figure S5). Zeta potential data of CDs solutions with different pH values (Figure S6). Thickness values of three representative films by profilometric method (Figure S7). Cross-sectional FESEM image of film (Figure S8). pH-dependent PL emissions of CDs solutions (Figure S9). Excitation-independent emissions of triluminous films (Figure S10). Photostability study of representative film at 275 nm (Figure S11). Decay lifetime spectra of CDs in ethanol (Figure S12). (PDF)

■ AUTHOR INFORMATION

Corresponding Author

*E-mail: gde@cgcri.res.in. Fax: +91 33 24730957. Tel: +91 33 23223403.

ORCID

Manish Kumar Mishra: 0000-0002-2901-628X

Goutam De: 0000-0003-0271-1634

Author Contributions

†D.B. and M.K.M. contributed equally.

Notes

The authors declare no competing financial interest.

■ ACKNOWLEDGMENTS

D.B. and M.K.M. thank CSIR, India for a senior research associateship under Scientists' Pool scheme and research fellowship, respectively. CSIR is acknowledged for support (project no. ESC0202).

■ REFERENCES

(1) Xu, X.; Ray, R.; Gu, Y.; Ploehn, H. J.; Gearheart, L.; Raker, K.; Scrivens, W. A. Electrophoretic Analysis and Purification of Fluorescent Single-Walled Carbon Nanotube Fragments. *J. Am. Chem. Soc.* **2004**, *126*, 12736−12737.

(2) Baker, S. N.; Baker, G. A. Luminescent Carbon Nanodots: Emergent Nanolights. *Angew. Chem., Int. Ed.* **2010**, *49*, 6726−6744.

(3) Wang, Y.; Kalytchuk, S.; Wang, L.; Zhovtiuk, O.; Cepe, K.; Zboril, R.; Rogach, A. L. Carbon Dot Hybrids with Oligomeric Silsesquioxane: Solid-State Luminophores with High Photoluminescence Quantum Yield and Applicability in White Light Emitting Devices. *Chem. Commun.* **2015**, *51*, 2950−2953.

(4) Xie, Z.; Wang, F.; Liu, C. Organic−Inorganic Hybrid Functional Carbon Dot Gel Glasses. *Adv. Mater.* **2012**, *24*, 1716−1721.
(5) Wang, X.; Cao, L.; Yang, S. T.; Lu, F.; Meziani, M. J.; Tian, L.; Sun, K. W.; Bloodgood, M. A.; Sun, Y. P. Bandgap-Like Strong Fluorescence in Functionalized Carbon Nanoparticles. *Angew. Chem., Int. Ed.* **2010**, *49*, 5310−5314.
(6) Nie, H.; Li, M.; Li, Q.; Liang, S.; Tan, Y.; Sheng, L.; Shi, W.; Zhang, S. X. Carbon Dots with Continuously Tunable Full-Color Emission and Their Application in Ratiometric pH Sensing. *Chem. Mater.* **2014**, *26*, 3104−3112.
(7) Zhu, S.; Zhang, J.; Tang, S.; Qiao, C.; Wang, L.; Wang, H.; Liu, X.; Li, B.; Li, Y.; Yu, W.; et al. Surface Chemistry Routes to Modulate the Photoluminescence of Graphene Quantum Dots: From Fluorescence Mechanism to Up-Conversion Bioimaging Applications. *Adv. Funct. Mater.* **2012**, *22*, 4732−4740.
(8) Zhu, S.; Meng, Q.; Wang, L.; Zhang, J.; Song, Y.; Jin, H.; Zhang, K.; Sun, H.; Wang, H.; Yang, B. Highly Photoluminescent Carbon Dots for Multicolor Patterning, Sensors, and Bioimaging. *Angew. Chem., Int. Ed.* **2013**, *52*, 3953−3957.
(9) Bao, L.; Liu, C.; Zhang, Z. L.; Pang, D. W. Photoluminescence-Tunable Carbon Nanodots: Surface-State Energy-Gap Tuning. *Adv. Mater.* **2015**, *27*, 1663−1667.
(10) Yang, C.; Zhu, S.; Li, Z.; Li, Z.; Chen, C.; Sun, L.; Tang, W.; Liu, R.; Sun, Y.; Yu, M. Nitrogen-Doped Carbon Dots with Excitation-Independent Long-Wavelength Emission Produced by a Room-Temperature Reaction. *Chem. Commun.* **2016**, *52*, 11912−11914.
(11) Qu, S.; Zhou, D.; Li, D.; Ji, W.; Jing, P.; Han, D.; Liu, L.; Zeng, H.; Shen, D. Toward Efficient Orange Emissive Carbon Nanodots through Conjugated sp^2-Domain Controlling and Surface Charges Engineering. *Adv. Mater.* **2016**, *28*, 3516−3521.
(12) Jiang, K.; Sun, S.; Zhang, L.; Lu, Y.; Wu, A.; Cai, C.; Lin, H. Red, Green and Blue Luminescence by Carbon Dots: Full-Color Emission Tuning and Multicolor Cellular Imaging. *Angew. Chem., Int. Ed.* **2015**, *54*, 5360−5363.
(13) Ding, H.; Yu, S. B.; Wei, J. S.; Xiong, H. M. Full-Color Light-Emitting Carbon Dots with a Surface-State-Controlled Luminescence Mechanism. *ACS Nano* **2016**, *10*, 484−491.
(14) Jiang, K.; Sun, S.; Zhang, L.; Wang, Y.; Cai, C.; Lin, H. Bright-Yellow-Emissive N-Doped Carbon Dots: Preparation, Cellular Imaging, and Bifunctional Sensing. *ACS Appl. Mater. Interfaces* **2015**, *7*, 23231−23238.
(15) Wang, H.; Sun, C.; Chen, X.; Zhang, Y.; Colvin, V. L.; Rice, Q.; Seo, J.; Feng, S.; Wang, S.; Yu, W. W. Excitation Wavelength Independent Visible Color Emission of Carbon Dots. *Nanoscale* **2017**, *9*, 1909−1915.
(16) Pramanik, S.; Bhandari, S.; Roy, S.; Chattopadhyay, A. Synchronous Tricolor Emission-Based White Light from Quantum Dot Complex. *J. Phys. Chem. Lett.* **2015**, *6*, 1270−1274.
(17) Wang, Y.; Kalytchuk, S.; Zhang, Y.; Shi, H.; Kershaw, S. V.; Rogach, A. L. Thickness-Dependent Full-Color Emission Tunability in a Flexible Carbon Dot Ionogel. *J. Phys. Chem. Lett.* **2014**, *5*, 1412−1420.
(18) Liu, X.; Pang, J.; Xu, F.; Zhang, X. Simple Approach to Synthesize Amino-Functionalized Carbon Dots by Carbonization of Chitosan. *Sci. Rep.* **2016**, *6*, 31100.
(19) Kwon, W.; Lee, G.; Do, S.; Joo, T.; Rhee, S. W. Size-Controlled Soft-Template Synthesis of Carbon Nanodots toward Versatile Photoactive Materials. *Small* **2014**, *10*, 506−513.
(20) Jiang, Z. C.; Lin, T. N.; Lin, H. T.; Talite, M. J.; Tzeng, T. T.; Hsu, C. L.; Chiu, K. P.; Lin, C. A. J.; Shen, J. L.; Yuan, C. T. A Facile and Low-Cost Method to Enhance the Internal Quantum Yield and External Light-Extraction Efficiency for Flexible Light Emitting Carbon-Dot Films. *Sci. Rep.* **2016**, *6*, 19991.
(21) Wang, D.; Liu, J.; Chen, J.; Dai, L. Surface Functionalization of Carbon Dots with Polyhedral Oligomeric Silsesquioxane (POSS) for Multifunctional Applications. *Adv. Mater. Interfaces* **2016**, *3*, 1500439.
(22) Kim, T. H.; Wang, F.; McCormick, P.; Wang, L.; Brown, C.; Li, Q. Salt-Embedded Carbon Nanodots as a UV and Thermal Stable Fluorophore for Light-Emitting Diodes. *J. Lumin.* **2014**, *154*, 1−7.
(23) Liu, Y.; Wang, P.; Fernando, K. A. S; LeCroy, G. E.; Maimaiti, H.; Harruff-Miller, B. A.; Lewis, W. K.; Bunker, C. E.; Hou, Z. L.; Sun, Y. P. Enhanced Fluorescence Properties of Carbon Dots in Polymer Films. *J. Mater. Chem. C* **2016**, *4*, 6967−6974.
(24) Bhunia, S. K.; Nandi, S.; Shikler, R.; Jelinek, R. Tuneable Light-Emitting Carbon-Dot/Polymer Flexible Films Prepared Through One-Pot Synthesis. *Nanoscale* **2016**, *8*, 3400−3406.
(25) Bullen, C.; Mulvaney, P.; Sada, C.; Ferrari, M.; Chiasera, A.; Martucci, A. Incorporation of a Highly Luminescent Semiconductor Quantum Dot in ZrO_2−SiO_2 Hybrid Sol−Gel Glass Film. *J. Mater. Chem.* **2004**, *14*, 1112−1116.
(26) Li, F.; Tian, F.; Liu, C.; Wang, Z.; Du, Z.; Li, R.; Zhang, L. One-Step Synthesis of Nanohybrid Carbon Dots and TiO_2 Composites with Enhanced Ultraviolet Light Active Photocatalysis. *RSC Adv.* **2015**, *5*, 8389−8396.
(27) Mishra, M. K.; De, G. Fabrication of $Cd_{0.5}Zn_{0.5}S$: Cu QDs Incorporated Organically Modified SiO_2 Films Showing Entire Visible Colour Emission with High Quantum Yield. *J. Mater. Chem. C* **2013**, *1*, 4816−4820.
(28) Vassilakopoulou, A.; Georgakilas, V.; Vainos, N.; Koutselas, I. Successful Entrapment of Carbon Dots within Flexible Free-Standing Transparent Mesoporous Organic-Inorganic Silica Hybrid Films for Photonic Applications. *J. Phys. Chem. Solids* **2017**, *103*, 190−196.
(29) Zhou, D.; Li, D.; Jing, P.; Zhai, Y.; Shen, D.; Qu, S.; Rogach, A. L. Conquering Aggregation-Induced Solid-State Luminescence Quenching of Carbon Dots through a Carbon Dots-Triggered Silica Gelation Process. *Chem. Mater.* **2017**, *29*, 1779−1787.
(30) Mishra, M. K.; Chakravarty, A.; Bhowmik, K.; De, G. Carbon Nanodot−ORMOSIL Fluorescent Paint and Films. *J. Mater. Chem. C* **2015**, *3*, 714−719.
(31) Mishra, M. K.; Kundu, S.; De, G. Stable fluorescent CdS: Cu QDs and Their Hybridization with Carbon Polymer Dots for White Light Emission. *J. Mater. Chem. C* **2016**, *4*, 1665−1674.
(32) Wang, F.; Xie, Z.; Zhang, H.; Liu, C. Y.; Zhang, Y. G. Highly Luminescent Organosilane-Functionalized Carbon Dots. *Adv. Funct. Mater.* **2011**, *21*, 1027−1031.
(33) Medda, S. K.; De, G. Inorganic−Organic Nanocomposite Based Hard Coatings on Plastics Using In Situ Generated Nano-SiO_2 Bonded with ≡Si—O—Si—PEO Hybrid Network. *Ind. Eng. Chem. Res.* **2009**, *48*, 4326−4333.
(34) Lü, C.; Yang, B. High Refractive Index Organic−Inorganic Nanocomposites: Design, Synthesis and Application. *J. Mater. Chem.* **2009**, *19*, 2884−2901.
(35) Vedamalai, M.; Periasamy, A. P.; Wang, C. W.; Tseng, Y. T.; Ho, L. C.; Shih, C. C.; Chang, H. T. Carbon Nanodots Prepared from *o*-Phenylenediamine for Sensing of Cu^{2+} Ions in Cells. *Nanoscale* **2014**, *6*, 13119−13125.
(36) Jiang, K.; Sun, S.; Zhang, L.; Wang, Y.; Cai, C.; Lin, H. Bright-Yellow-Emissive N Doped Carbon Dots: Preparation, Cellular Imaging, and Bifunctional Sensing. *ACS Appl. Mater. Interfaces* **2015**, *7*, 23231−23238.
(37) Wang, B. B.; Cheng, Q. J.; Wang, L. H.; Zheng, K.; Ostrikov, K. The Effect of Temperature on the Mechanism of Photoluminescence from Plasma-Nucleated, Nitrogenated Carbon Nanotips. *Carbon* **2012**, *50*, 3561−3571.
(38) Park, S. S.; Chu, S. W.; Xue, C.; Zhao, D.; Ha, C. S. Facile Synthesis of Mesoporous Carbon Nitrides using the Incipient Wetness Method and the Application as Hydrogen Adsorbent. *J. Mater. Chem.* **2011**, *21*, 10801−10807.
(39) Kaczor, A.; Szczepanski, J.; Vala, M.; Kozłowski, H.; Proniewicz, L. M. Infrared Absorption Spectra of 2-(Hydroxyimino) Propanohydroxamic and Oxalodihydroxamic Acids Isolated in Argon Matrices. *Phys. Chem. Chem. Phys.* **2003**, *5*, 2337−2343.
(40) Richards, R. F.; Thompson, H. W. Spectroscopic Studies of the Amide Linkage. *J. Chem. Soc.* **1947**, *237*, 1248.
(41) Higgins, F. S.; Magliocco, L. G.; Colthup, N. B. Infrared and Raman Spectroscopy Study of Alkyl Hydroxamic Acid and Alkyl Hydroxamate Isomers. *Appl. Spectrosc.* **2006**, *60*, 279−287.

DOI: 10.1021/acs.jpcc.7b08039
J. Phys. Chem. C 2017, 121, 28106−28116

(42) Zhang, Y.; Liu, X.; Fan, Y.; Guo, X.; Zhou, L.; Lv, Y.; Lin, J. One-Step Microwave Synthesis of N-doped Hydroxyl-Functionalized Carbon Dots with Ultra-High Fluorescence Quantum Yields. *Nanoscale* **2016**, *8*, 15281−15287.
(43) Chakravarty, A.; Bhowmik, K.; De, G.; Mukherjee, A. Synthesis of Amine Functionalized Graphite Nanosheets and Their Water-Soluble Derivative for Drug Loading and Controlled Release. *New J. Chem.* **2015**, *39*, 2451−2458.
(44) Li, Q.; Yang, J.; Feng, D.; Wu, Z.; Wu, Q.; Park, S. S.; Ha, C. S.; Zhao, D. Facile Synthesis of Porous Carbon Nitride Spheres with Hierarchical Three-Dimensional Mesostructures for CO_2 Capture. *Nano Res.* **2010**, *3*, 632−642.
(45) Vinu, A. Two-Dimensional Hexagonally-Ordered Mesoporous Carbon Nitrides with Tunable Pore Diameter, Surface Area and Nitrogen Content. *Adv. Funct. Mater.* **2008**, *18*, 816−827.
(46) Artyushkova, K.; Levendosky, S.; Atanassov, P.; Fulghum, J. XPS Structural Studies of Nano-composite Non-platinum Electrocatalysts for Polymer Electrolyte Fuel Cells. *Top. Catal.* **2007**, *46*, 263−275.
(47) Xiong, X.; Kang, Y.; Yang, G.; Zhang, S.; Yu, L.; Zhang, P. Preparation and Evaluation of Tribological Properties of Cu Nanoparticles Surface Modified by Tetradecyl Hydroxamic Acid. *Tribol. Lett.* **2012**, *46*, 211−220.
(48) Fan, X.; Peng, W.; Li, Y.; Li, X.; Wang, S.; Zhang, G.; Zhang, F. Deoxygenation of Exfoliated Graphite Oxide Under Alkaline Conditions: a Green Route to Graphene Preparation. *Adv. Mater.* **2008**, *20*, 4490−4493.
(49) Zhao, H.; Chen, X.; Jia, C.; Zhou, T.; Qu, X.; Jian, J.; Xu, Y.; Zhou, T. A Facile Mechanochemical Way to Prepare g-C_3N_4. *Mater. Sci. Eng., B* **2005**, *122*, 90−93.
(50) Shao, Y.; Zhang, S.; Engelhard, M. H.; Li, G.; Shao, G.; Wang, Y.; Liu, J.; Aksay, I. A.; Lin, Y. Nitrogen-Doped Graphene and Its Electrochemical Applications. *J. Mater. Chem.* **2010**, *20*, 7491−7496.
(51) Morant, C.; Torres, R.; Jimenez, I.; Sanz, J. M.; Elizalde, E. Characterization of Nitrogen-Doped Carbon Nanotubes by Atomic Force Microscopy, X-ray Photoelectron Spectroscopy and X-ray Absorption Near Edge Spectroscopy. *J. Nanosci. Nanotechnol.* **2009**, *9*, 3633−3638.
(52) Chua, C. K.; Sofer, Z.; Simek, P.; Jankovsky, O.; Klimova, K.; Bakardjieva, S.; Kuckova, S. H.; Pumera, M. Synthesis of Strongly Fluorescent Graphene Quantum Dots by Cage-Opening Buckminsterfullerene. *ACS Nano* **2015**, *9*, 2548−2555.
(53) Buglass, A. J.; Hudson, K.; Tillett, J. G. The Acid-Catalysed Hydrolysis and Protonation Behaviour of Hydroxamic Acids. *J. Chem. Soc. B* **1971**, *0*, 123−126.
(54) García, B.; Ibeas, S.; Hoyuelos, F. J.; Leal, J. M.; Secco, F.; Venturini, M. Hydroxamic Acids as Weak Base Indicators: Protonation in Strong Acid Media. *J. Org. Chem.* **2001**, *66*, 7986−7993.
(55) Oh, H. K.; Ku, M. H.; Lee, H. W.; Lee, I. Kinetics and Mechanism of the Pyridinolysis of Aryl Furan-2-carbodithioates in Acetonitrile. *J. Org. Chem.* **2002**, *67*, 8995−8998.
(56) Lipczynska-Kochany, E.; Iwamura, H. Oxygen-17 Nuclear Magnetic Resonance Studies of the Structures of Benzohydroxamic Acids and Benzohydroxamate Ions in Solution. *J. Org. Chem.* **1982**, *47*, 5277−5282.
(57) Shi, S.; Jia, J.; Guo, X.; Zhao, Y.; Chen, D.; Guo, Y.; Cheng, T.; Zhang, X. Biocompatibility of Chitosan-Coated Iron Oxide Nanoparticles with Osteoblast Cells. *Int. J. Nanomed.* **2012**, *7*, 5593−5602.
(58) Wang, W. J.; Xia, J.; Feng, J.; He, M.; Chen, M. L.; Wang, J. H. Green Preparation of Carbon Dots for Intracellular pH Sensing and Multicolor Live Cell Imaging. *J. Mater. Chem. B* **2016**, *4*, 7130−7137.
(59) Bordwell, F. G.; Fried, H. E.; Hughes, D. L.; Lynch, T.-Y.; Satish, A. V.; Whang, Y. E. Acidities of Carboxamides, Hydroxamic Acids, Carbohydrazides, Benzenesulfonamides, and Benzenesulfonohydrazides in DMSO Solution. *J. Org. Chem.* **1990**, *55*, 3330−3336.
(60) Ventura, O. N.; Rama, J. B.; Turi, L.; Dannenberg, J. J. Acidity of Hydroxamic Acids: An ab Initio and Semiempirical Study. *J. Am. Chem. Soc.* **1993**, *115*, 5754−5761.
(61) Permatasari, F. A.; Aimon, A.; Iskandar, H. F.; Ogi, T.; Okuyama, K. Role of C−N Configurations in the Photoluminescence of Graphene Quantum Dots Synthesized by a Hydrothermal Route. *Sci. Rep.* **2016**, *6*, 21042.
(62) Wang, L.; Zhu, S.-J.; Wang, H.-Y.; Qu, S.-N.; Zhang, Y.-L.; Zhang, J.-H.; Chen, Q.-D.; Xu, H.-L.; Han, W.; Yang, B.; et al. Common Origin of Green Luminescence in Carbon Nanodots and Graphene Quantum Dots. *ACS Nano* **2014**, *8*, 2541−2547.
(63) Zhu, S.; Zhang, J.; Tang, S.; Qiao, C.; Wang, L.; Wang, H.; Liu, X.; Li, B.; Li, Y.; Yu, W.; et al. Surface Chemistry Routes to Modulate the Photoluminescence of Graphene Quantum Dots: From Fluorescence Mechanism to Up-Conversion Bioimaging Applications. *Adv. Funct. Mater.* **2012**, *22*, 4732−4740.
(64) Lu, S.; Zhao, X.; Zhu, S.; Song, Y.; Yang, B. Novel Cookie-with-Chocolate Carbon Dots Displaying Extremely Acidophilic High Luminescence. *Nanoscale* **2014**, *6*, 13939−13944.
(65) Dong, Y.; Pang, H.; Yang, H. B.; Guo, C.; Shao, J.; Chi, Y.; Li, C. M.; Yu, T. Carbon-Based Dots Co-doped with Nitrogen and Sulfur for High Quantum Yield and Excitation-Independent Emission. *Angew. Chem., Int. Ed.* **2013**, *52*, 7800−7804.
(66) Dhenadhayalan, N.; Lin, K.; Suresh, R.; Ramamurthy, P. Unravelling the Multiple Emissive States in Citric-Acid-Derived Carbon Dots. *J. Phys. Chem. C* **2016**, *120*, 1252−1261.
(67) Bao, L.; Zhang, Z. L.; Tian, Z. Q.; Zhang, L.; Liu, C.; Lin, Y.; Qi, B.; Pang, D. W. Electrochemical Tuning of Luminescent Carbon Nanodots: From Preparation to Luminescence Mechanism. *Adv. Mater.* **2011**, *23*, 5801−5806.
(68) Yu, P.; Wen, X.; Toh, Y. R.; Tang, J. Temperature-Dependent Fluorescence in Carbon Dots. *J. Phys. Chem. C* **2012**, *116*, 25552−25557.

NOTE ADDED AFTER ASAP PUBLICATION

This paper was published to the Web on December 11, 2017, with errors in Figure 1. These were corrected in the version published to the Web on December 13, 2017.

DOI: 10.1021/acs.jpcc.7b08039
J. Phys. Chem. C 2017, 121, 28106−28116